Susceptibility of aerosol optical thickness retrievals to thin cirrus contamination during the BASE-ASIA campaign

Jingfeng Huang,[1,2] N. Christina Hsu,[2] Si-Chee Tsay,[2] Myeong-Jae Jeong,[1,2,3] Brent N. Holben,[2] Timothy A. Berkoff,[1,2] and Ellsworth J. Welton[2]

Received 16 August 2010; revised 26 January 2011; accepted 8 February 2011; published 30 April 2011.

[1] We used a combination of ground measurements (Aerosol Robotic Network, AERONET; Micro-Pulse Lidar Network, MPLNET) and satellite data (Moderate Resolution Imaging Spectroradiometer, MODIS; Cloud-Aerosol Lidar and Infrared Pathfinder Satellite Observation, CALIPSO) to examine the susceptibility of ground and satellite aerosol retrievals to thin cirrus contamination at Phimai, Thailand (102.56°E, 15.18°N, also known as Pimai), during the Biomass-burning Aerosols in South East-Asia: Smoke Impact Assessment (BASE-ASIA) campaign (February–May 2006). Using the strengths of spaceborne or ground lidars to detect cirrus clouds, we conducted statistical analyses for four different scenarios: MPLNET versus AERONET, MPLNET versus MODIS, CALIPSO versus AERONET, and CALIPSO versus MODIS. Cirrus identifications from MPLNET or CALIPSO were paired up with concurrent aerosol optical thickness (AOT) measurements from AERONET or MODIS. Results from the BASE-ASIA campaign suggest that current operational AERONET and MODIS AOT products are influenced by thin cirrus contamination featuring strong seasonality. Concurrent AERONET and MPLNET observations indicate that additional thin cirrus screening changes AOT monthly means by 5%, with 20% of the AERONET aerosol data at Phimai being cirrus contaminated in boreal spring. From noncirrus cases to cirrus-contaminated cases, AERONET AOT increases along with larger particle sizes. We further evaluated the performance of eight MODIS-derived cirrus screening parameters for their effectiveness on thin cirrus screening: apparent reflectance at 1.38 μm (R1.38), cirrus reflectance at 0.66 μm (CR0.66), CR0.66 cirrus flag, reflectance ratio between 1.38 μm and 0.66 μm (RR1.38/0.66), reflectance ratio between 1.38 μm and 1.24 μm (RR1.38/1.24), brightness temperature difference between 8.6 μm and 11 μm (BTD8.6–11), brightness temperature difference between 11 μm and 12 μm (BTD11–12), and cloud phase infrared approach. Correlation analysis with the MPLNET cirrus flag indicates that RR1.38/0.66 is slightly preferable for high thin cirrus screening for the AERONET AOT measurements. The quantitative findings from this study suggest particular caution and careful evaluation of thin cirrus contamination in the satellite and ground AOT measurements before they are used for aerosol-related climatic forcing studies.

Citation: Huang, J., N. C. Hsu, S.-C. Tsay, M.-J. Jeong, B. N. Holben, T. A. Berkoff, and E. J. Welton (2011), Susceptibility of aerosol optical thickness retrievals to thin cirrus contamination during the BASE-ASIA campaign, *J. Geophys. Res.*, *116*, D08214, doi:10.1029/2010JD014910.

1. Introduction

[2] Due to the diversity of its aerosol types, large variability in its aerosol loading, and its unique maritime continental environment, Southeast Asia has been a region of interest for aerosol-related scientific studies [e.g., *Breon et al.*, 2002; *Hsu et al.*, 1996, 2003; *Menon et al.*, 2002; *Hsu et al.*, 2006]. Biomass burning smoke, dust and industrial pollution are frequently observed in the region [e.g., *Chu et al.*, 2003; *Levine et al.*, 1989]; however, the aerosol and cloud/precipitation interactions and thus their climatic impacts are still poorly understood [e.g., *Andreae*, 1991; *Hansell et al.*, 2003; *Hsu et al.*, 2003; *Luo*, 2004; *Li et al.*, 2007; *Unger et al.*, 2009]. Model simulations and observational evidence are not always consistent with each other on the large-scale aerosol effects [e.g., *Takemura et al.*, 2005; *Tao et al.*, 2007], which may be attributed to large uncertainties associated with model parameterizations [e.g., *Takemura et al.*, 2005] or satellite remote sensing retrieval algorithms

[1]Goddard Earth Sciences and Technology Center, University of Maryland Baltimore County, Baltimore, Maryland, USA.
[2]NASA Goddard Space Flight Center, Greenbelt, Maryland, USA.
[3]Now at Department of Atmospheric and Environmental Sciences, Gangneung-Wonju National University, Gangneung, South Korea.

Copyright 2011 by the American Geophysical Union.
0148-0227/11/2010JD014910

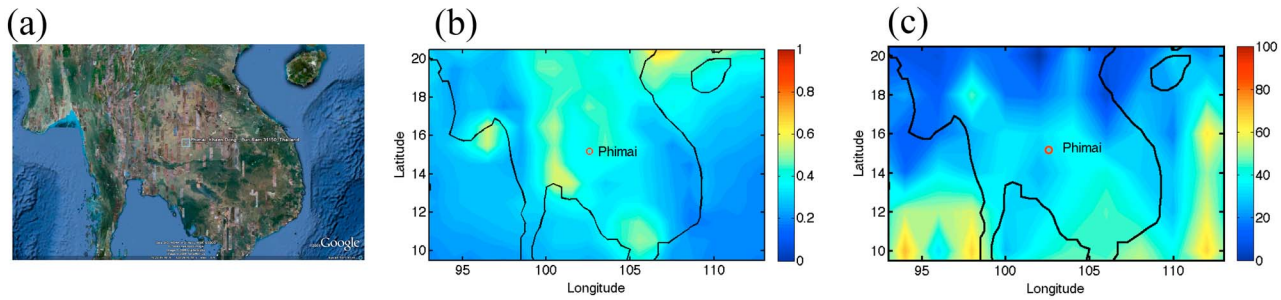

Figure 1. (a) Geographical location of Phimai (102.56°E, 15.18°N) (Google Earth); (b) monthly mean of Aqua MODIS AOT during BASE-ASIA campaign, February–May 2006; and (c) thin cirrus occurrence frequency (%) during February–May 2007, as observed by CALIPSO.

[e.g., *Myhre et al.*, 2005; *Jeong et al.*, 2005; *Jeong and Li*, 2005].

[3] One of the key difficulties for aerosol retrieval in Southeast Asia is the persistent occurrence of high thin cirrus clouds that need to be completely removed by cloud screening schemes [*Gao et al.*, 2002a, 2002b; *Kaufman et al.*, 2005; *Lee et al.*, 2009; *Meyer and Platnick*, 2010]. Consequently, unscreened thin cirrus results in aerosol optical thickness (AOT) high bias due to data contamination. In order to accurately quantify the climate forcing of aerosols in this region, it is necessary to perform rigorous and systematic evaluations to determine the degree of cirrus contamination in both ground based and satellite aerosol products and to investigate better alternatives for thin cirrus screening schemes.

[4] With the advent of the A-Train satellite constellation, comprehensive measurements of global cirrus cloud coverage and its temporal and spatial variability have become available for the first time in recent years [*Sassen et al.*, 2008; *Massie et al.*, 2010]. As part of the A-Train, the cloud-aerosol lidar with orthogonal polarization (CALIOP) sensor onboard Cloud-Aerosol Lidar and Infrared Pathfinder Satellite Observation (CALIPSO) provides important information on the vertical distributions of aerosol and cloud layers from space. In addition, the Moderate Resolution Imaging Spectroradiometer (MODIS) has a unique 1.38 μm channel, that is also valuable for cirrus detection purposes [*Gao and Kaufman*, 1995]. Owing to its strong water vapor absorption, the 1.38 μm channel is more sensitive to upper tropospheric clouds than to low-level clouds [*Gao and Kaufman*, 1995]. Because cirrus clouds usually occur at higher altitude (>10 km in the tropical region) and are mostly associated with ice clouds, various techniques of cirrus detection based on apparent reflectance at the 1.38 μm, brightness temperature difference in thermal IR channels and their combinations have been investigated in previous studies [*Gao and Kaufman*, 1995; *Gao et al.*, 2002a, 2002b; *Roskovensky and Liou*, 2003; *Lee et al.*, 2009; *Meyer and Platnick*, 2010]. However, these studies have not quantitatively examined these parameters in relation to ground or spaceborne lidar data for cirrus screening purposes.

[5] In this paper, we systematically investigate the effects of thin cirrus contamination in ground based and satellite retrieved aerosol products by taking advantage of the lidar measurements acquired during the Biomass-burning Aerosols in South East-Asia: Smoke Impact Assessment (BASE-ASIA) field campaign conducted at Phimai, Thailand, (102.56°E, 15.18°N; see Figure 1a), during February–May in 2006. The mean AOT at Phimai over this biomass burning season was moderate (i.e., ~0.4 as derived from Aqua MODIS in Figure 1b). Unfortunately, CALIPSO data is only available after Jun 2006, not covering the BASE-ASIA period. The thin cirrus occurrence frequency during same season (February–May) in 2007 was about 40% as observed by CALIPSO (Figure 1c). During the campaign, significant ground-based measurements were obtained by various instruments in the NASA SMART (Surface-sensing Measurements for Atmospheric Radiative Transfer) and COMMIT (Chemical, Optical & Microphysical Measurements of In situ Troposphere) facilities (http://smart.gsfc.nasa.gov/). The field campaign provided an excellent opportunity to look into the issue of cirrus identification and its contamination to aerosol measurements, by providing aerosol measurements concurrently with comprehensive cloud information.

[6] Based on the data sets from the BASE-ASIA campaign and operational satellites, this study aims to (1) investigate the susceptibility of AOT measurements to cirrus contamination and quantify its influence; (2) evaluate the performance of several satellite retrieved cirrus screening parameters; and (3) propose appropriate cirrus screening parameter from operational satellite based on its efficiency and effectiveness. Data descriptions are given in section 2, followed by results demonstration in section 3. Section 4 summarizes our main findings and conclusions.

2. Data and Data Processing

[7] In this study, we use aerosol retrievals from the Aerosol Robotic Network (AERONET) and MODIS products, while lidar data from the Micro-Pulse Lidar Network (MPLNET) and CALIPSO play a key role in our cirrus cloud identification scheme. For cirrus screening parameters, we evaluate multiple parameters from the MODIS L1B and cloud products.

2.1. AERONET

[8] AERONET provides a long-term, continuous and readily accessible database of aerosol optical, microphysical and radiative properties for aerosol research and characterization, validation of satellite retrievals, and synergism with

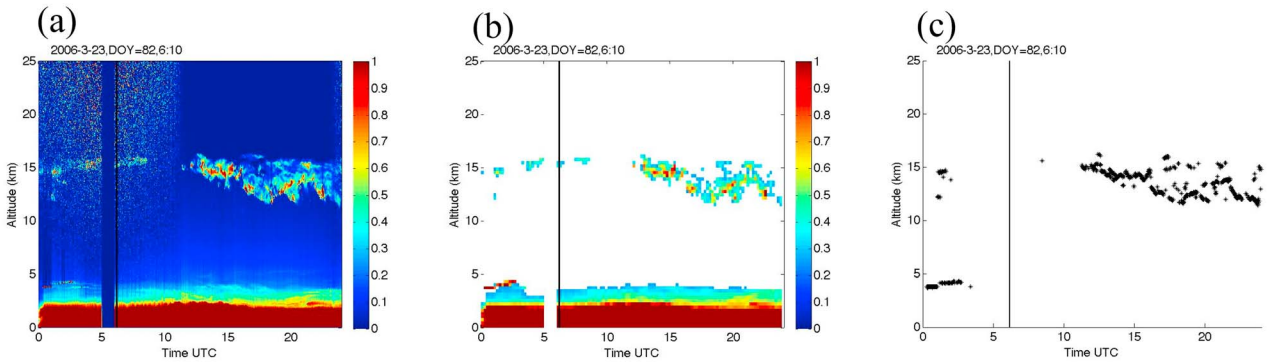

Figure 2. MPLNET (a) L1.0 normalized relative backscatter (NRB), (b) L1.0 cirrus flag (CF), and (c) L1.5b cloud base height (CB). Vertical lines denote Aqua MODIS overpass time on 23 March 2006.

other databases [*Holben et al.*, 1998] (http://aeronet.gsfc.nasa.gov). For this study, we used the AERONET Level 2.0 (cloud-screened and quality-assured, in the version 2 direct sun algorithm product) AOT (500 nm) data taken at Phimai during the BASE-ASIA period. To investigate changes in particle size attributable to cirrus contamination, we also used the aerosol size distribution and Angstrom Exponent data in AERONET version 2 inversion products. The L2.0 aerosol fine mode fraction in the AERONET version 2 direct sun algorithm products in 2006 was also used when its relationship to the collocated MODIS-derived thin cirrus parameters was studied.

[9] The current AERONET AOT cloud screening is based on examining temporal variability of measured AOT through a three-step approach [*Smirnov et al.*, 2000]. First, each reported observation consists of the mean of three consecutive measurements (triplet) over a 1 min time interval. If the triplet AOT variability is either larger than 0.02 or 0.03*AOT (whichever is larger), the data are classified as cloudy. Then for daily intervals, if the standard deviation of the remaining AOT (500 nm) data points is still higher than 0.015, the smoothness of the temporal variability of AOT for the day is tested and observations with the temporal variability beyond certain threshold values will be discarded as cloudy. Finally, at each day, any observations of AOT (500 nm) and Angstrom exponent residing beyond the 3 standard deviations within the daily intervals are also removed from valid observations. While the AERONET method based on temporal variability works effectively for eliminating most cloud contaminated data, it could inadvertently eliminate some data influenced by variable aerosols like smoke plumes [e.g., *Kaufman et al.*, 2006]. On the other hand, some residual AOT observations contaminated by thin stable cirrus may fail to be screened out [e.g., *Kaufman et al.*, 2005; *Schaap et al.*, 2009], which warrant further investigations for this study.

2.2. MPLNET

[10] The NASA Micro-Pulse Lidar Network (MPLNET) provides continuous multiyear records of vertically resolved atmospheric measurements of aerosol and clouds at multiple sites around the globe. During the BASE-ASIA campaign, joint measurements from an MPLNET lidar and an AERONET Sun photometer in the SMART-COMMIT mobile facilities provide both column and vertically resolved aerosol and cloud data, such as: optical depth, single scatter albedo, size distribution, aerosol and cloud heights, planetary boundary layer (PBL) structure and evolution, and profiles of extinction and backscatter [*Welton et al.*, 2001; *Berkoff et al.*, 2008] (http://mplnet.gsfc.nasa.gov).

[11] In this study, the standard MPLNET data sets used are: (1) Level 1.0 normalized relative backscatter (L1.0 NRB), used primarily for cirrus visualization purpose; (2) Level 1.5b cloud base (L1.5b CB), used to verify the effectiveness of an enhanced cloud flag (L1.0 CF) developed in this work for automated cirrus identification.

[12] The L1.0 CF is generated based on statistical characterization of the MPLNET NRB data in each time-space window (300 m in range and 12 min in time). In order to minimize the influence from MPLNET daytime noise and simultaneously identify existence of cirrus cloud, the NRB data in each time-space window have to satisfy the following criteria to be flagged as cirrus: (1) the total number of samples has to exceed 35; (2) the averaged NRB value has to exceed 0.25; and (3) the cloud altitude has to be higher than 10 km. These threshold values are justified according to systematic inspections on the effective removal of daytime noise and successful identification of thin cirrus that are observed in the L1.0 NRB imagery.

[13] The effectiveness of the L1.0 CF approach in identifying cirrus clouds can be seen in its comparison to the L1.0 NRB and L1.5b CB products in Figure 2 for a very thin cirrus case on 23 March 2006. In addition to its capability of removing surrounding noises in the NRB daytime profile, it more effectively resembles the cloud features in the L1.0 NRB and the cloud base height in the L1.5b CB. This scheme also more successfully detects some very fine cloud features, for example such as the thin cirrus around 0600 UTC in Figure 2b, which are outstandingly present in the L1.0NRB but missed in the L1.5b CB.

2.3. MODIS

[14] The Terra and Aqua MODIS sensors provide wide range of multiwavelength atmospheric observations (http://modis-atmos.gsfc.nasa.gov/). For this study, because CALIPSO is only 1–2 min apart from Aqua MODIS and also because some Terra MODIS bands have a quality degradation issue after 2004, we only use the most updated AOT measurements

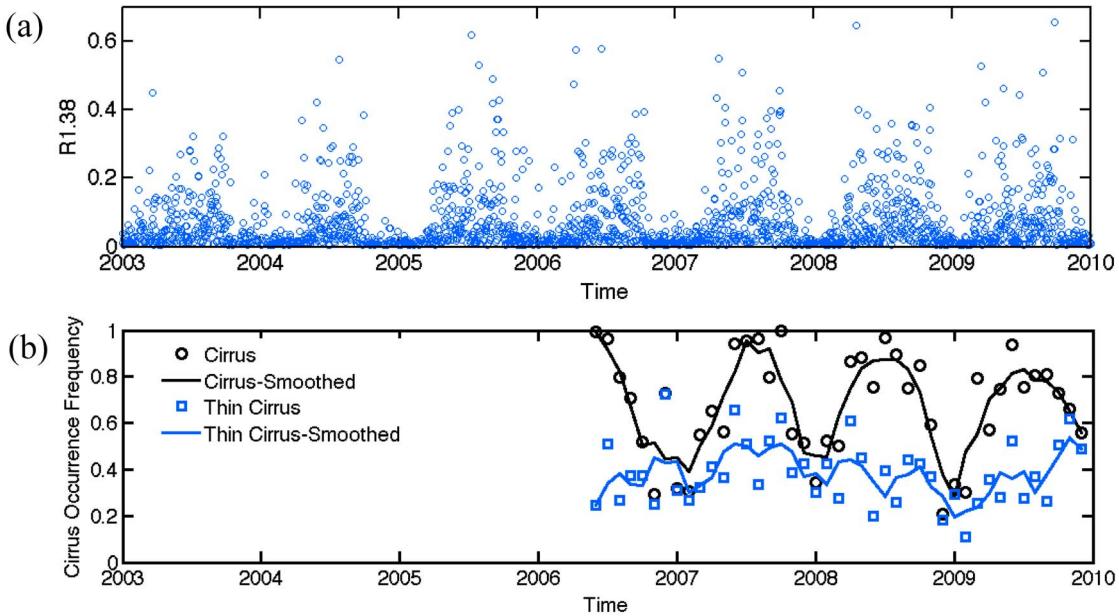

Figure 3. (a) Aqua MODIS daily R1.38 in a 1° × 1° box centered in Phimai (102°E–103°E, 15°N–16°N) from 2003 to 2009 and (b) CALIPSO observed monthly cirrus occurrence frequency in a 5° × 5° box centered in Phimai from June 2006 to February 2009. The thin cirrus occurrence is the CALIPSO cirrus occurrence constraint by Aqua MODIS R1.38 less than 0.02.

from Aqua MODIS to assure confidence in the cirrus screening parameter selection. However, the Terra-MODIS band 26 (1.38 μm) and band 1 (0.66 μm) that do not have quality degradation issues were still used when they were collocated with AERONET AOT measurements.

[15] In the MODIS Collection 5 aerosol retrievals over the vegetated surfaces (L. A. Remer et al., Algorithm for remote sensing of tropospheric aerosol from MODIS: Collection 005, 2009, http://modis-atmos.gsfc.nasa.gov) (hereinafter Remer et al., online publication, 2009), the cirrus screening scheme classifies 'cloudy' pixels if the standard deviations of the apparent reflectances at 0.47 μm (R0.47) and at 1.38 μm (R1.38) are higher than 0.0025 or 0.003, respectively, or the absolute values of R0.47 > 0.4 or R1.38 > 0.025. Additionally, those pixels with 0.01 < R1.38 < 0.025 are classified 'not cloudy but quality flag of aerosol retrieval is zero, QA = 0'; if R1.38 < 0.01, 'not cloudy and quality assured for thin cirrus screening.' So, for quality assured aerosol retrievals (QA = 3), R1.38 has to be less than 0.01. In other words, if a threshold value of R1.38 = 0.01 still results in residual thin cirrus contamination, it will influence the quality assured MODIS aerosol retrievals. To evaluate the robustness of R1.38 in thin cirrus screening, the CALIPSO and MPLNET lidar data are used to identify those possibly contaminated MODIS aerosol data.

[16] Besides the MODIS aerosol products MYD04_L2 [*Kaufman et al.*, 1997; *Hsu et al.*, 2006; Remer et al., online publication, 2009], we also examined eight MODIS retrieved parameters that are potentially useful for cirrus screening. They are: apparent reflectance at 1.38 μm (R1.38), its derivative cirrus reflectance at 0.66 μm (CR0.66), cirrus flag (CF), reflectance ratio between 1.38 μm and 0.66 μm (RR1.38/0.66), reflectance ratio between 1.38 μm and 1.24 μm (RR1.38/1.24), brightness temperature difference between 8.6 μm and 11 μm (BTD8.6–11), brightness temperature difference between 11 μm and 12 μm (BTD11–12), and cloud phase infrared approach (CPIR). R1.38, R0.66 and R1.24 are retrieved from the MODIS Level 1B 1km product, MYD021KM, and all the rest are in the MODIS Level 2 cloud products, MYD06_L2.

2.4. CALIPSO

[17] As part of the A-Train constellation, CALIPSO combines an active lidar instrument (CALIOP) with passive infrared and visible imagers to probe the vertical structure and properties of thin clouds and aerosols over the globe [*Vaughan et al.*, 2004].

[18] For this study, we utilize the Level 2.0 CALIPSO vertical feature mask (VFM) v2.01 covering June 2006 through September 2008 as a reference tool for cirrus cloud detection. The CALIPSO VFM provides aerosol and cloud layer heights along with aerosol and cloud types, including a 'transparent thin cirrus' subtype [*Vaughan et al.*, 2005; *Liu et al.*, 2009]. VFM v2.02 from October 2008 to December 2009 were also used for thin cirrus climatology purposes.

3. Results and Discussions

3.1. Cirrus Climatology at Phimai

[19] We first examined cirrus seasonality at Phimai by calculating daily R1.38 from the Aqua MODIS in the 1° × 1° grid centered at Phimai from 2003 to 2009 (Figure 3a). Similarly, we presented the cirrus identification from CALIPSO VFM as the black curve and markers in Figure 3b, covering June 2006 to December 2009. The seasonal cycle of cirrus as detected by CALIPSO is very similar to that found with MODIS R1.38, showing that the occurrence frequency

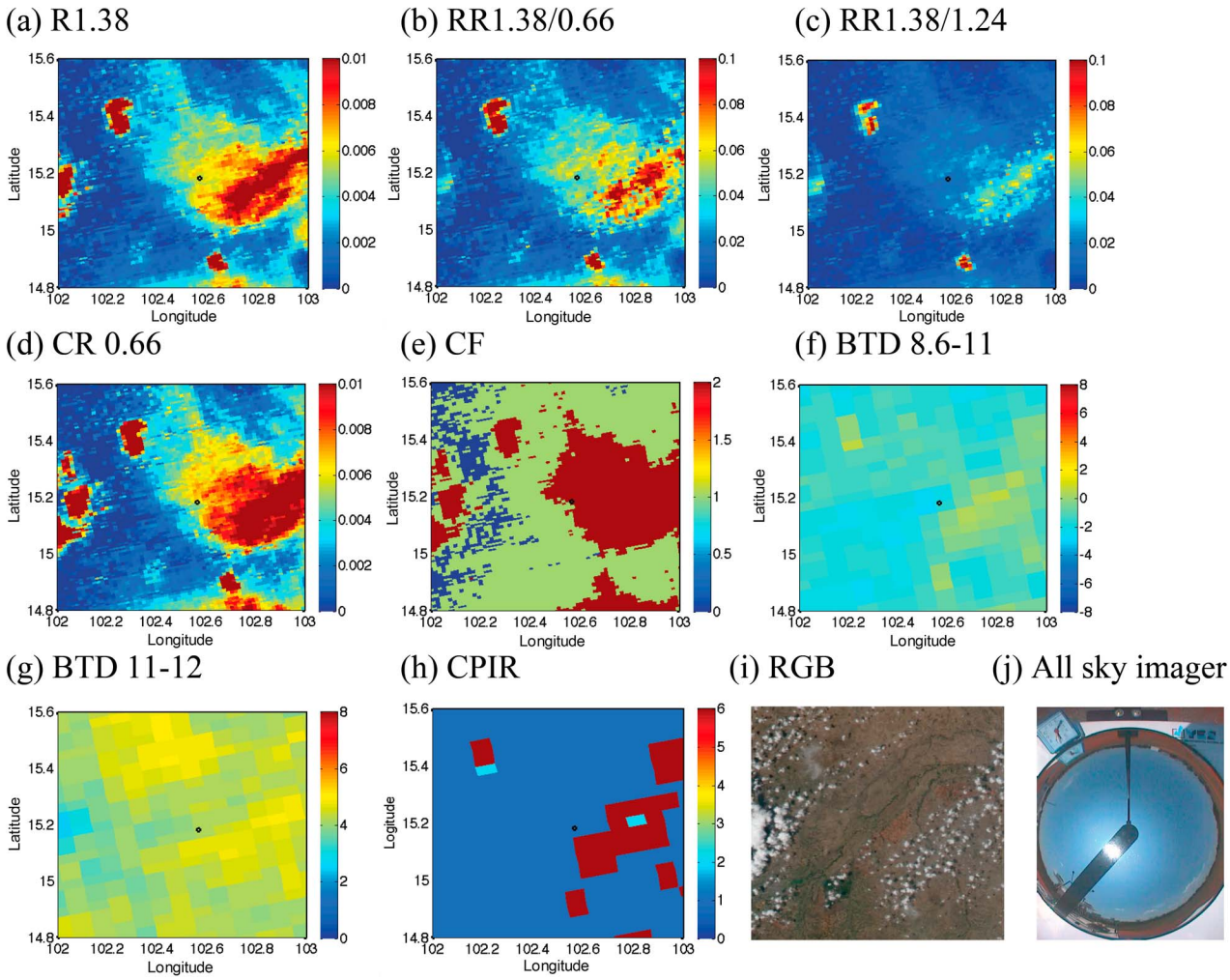

Figure 4. Images of eight Aqua MODIS-retrieved cirrus-screening parameters on 23 March 2006 in the region around Phimai: (a) R1.38, (b) RR1.38/0.66, (c) RR 1.38/1.24, (d) CR 0.66, (e) CF, (f) BTD 8.6–11, (g) BTD 11–12, and (h) CPIR. As references, the corresponding (i) true-color RGB image and (j) all sky imager are provided. A black circle near the center of the images denotes the location of Phimai.

of cirrus, a combination of both thin and thick cirrus, peaks in boreal summer and becomes less frequent in other seasons. Next, because cirrus thickness can be roughly indicated by the detection of surface return signal [*Sassen et al.*, 2008], by constraining the existence of surface return lidar signal onto CALIPSO cirrus identification, we estimated the seasonality of high thin cirrus (which optical thickness is usually low and thus allow the detection of surface return signal), shown as the blue curve and markers in Figure 3b. In contrast to total cirrus clouds, thin cirrus occur more often in boreal spring (such as the BASE-ASIA period) and autumn with two seasonal peaks. This is expected since convective activities are stronger over summer and result in much thicker cirrus clouds in monsoon season. However, in this study, we are more interested in thin cirrus, because this type of clouds is more transparent and difficult to be screened, the AERONET and MODIS AOT measurements during the BASE-ASIA period are potentially more vulnerable to thin cirrus contamination, which will be further demonstrated in section 3.3. As calculated from CALIPSO, the average altitude of cirrus clouds over Phimai from June 2006 to February 2009 is ~13 km.

3.2. Case Study of Cirrus Identification on 23 March 2006

[20] Before more quantitative analysis, we first present a thin cirrus case at Phimai on 23 March 2006 (Figure 4). From the MPLNET observations, we can clearly see persistent cirrus cloud feature in the NRB profile and the L1.0 CF when Aqua MODIS overpass (see Figures 2a and 2b). The corresponding values of the 8 MODIS-derived cirrus-screening parameters are listed in Table 1. From a comparison with the MODIS R1.38 and RGB images (Figures 4a and 4i, respectively), one can see that R1.38 is more sensitive to high clouds than to low clouds because it had much lower values in some low-cloud areas as seen in the RGB image and evident by their corresponding high R0.66 values (not shown). Thin cirrus around Phimai was subvisual in the RGB (Figure 4i), as well as the all sky imager (Figure 4j). The MODIS cirrus-screening

Table 1. Values of the Eight Aqua MODIS Cirrus-Screening Parameters at Phimai on 23 March 2006

	R1.38	RR1.38/0.66	RR1.38/1.24	CR0.66	CF	BTD 8.6–11	BTD 11–12	CPIR
Value	0.0055	0.0443	0.0170	0.0068	2 (cirrus)	−2.49	3.98	0 (clear)

parameters, including R1.38, RR1.38/0.66, RR1.38/1.24, CR0.66 and CF (Figures 4a, 4b, 4c, 4d and 4e, respectively), seem capable to discriminate thin cirrus from the nearby thick cirrus regions or cloud free regions depending on their threshold value selections, except BTD8.6–11, BTD11–12 and CPIR (Figures 4f, 4g and 4h, respectively). These three ice content related parameters were not very sensitive to the existence of this thin cirrus layer probably because the ice content in such thin cirrus was not sufficiently high. In order to screen thin cirrus cases like the one on 23 March 2006, threshold value of each parameter should be carefully selected which will be further addressed in section 3.4.

3.3. Investigations of Cirrus Contamination in Aerosol Retrievals

3.3.1. AERONET Versus MPLNET

[21] To evaluate possible cirrus contamination in the AERONET aerosol measurements during the BASE-ASIA period, we matched up the AERONET aerosol measurements with the MPLNET L1.0 CF in each 12 min time bin. Some basic statistical results are summarized as follows: First, in terms of cirrus occurrence frequency, over the 80 days of the BASE-ASIA campaign (February–May 2006), 1120 (23.3%) out of all 4800 MPL daytime (0000–1200 UTC) 12 min time bins were reported with cirrus by MPL L1.0 CF. Consistent with CALIPSO observations, the average altitude of these cirrus clouds is about 13 km; Second, in terms of the coincident occurrence of cirrus and AOT, out of the 732 AERONET AOT values simultaneously reported in the MPL daytime 12 min time bins, there were 177 (24.2%) of them were flagged with cirrus by MPL. In other words, cirrus may be observed at 20–25% chances at Phimai in boreal spring. And there are about 20–25% chances that the AERONET AOT measurements were possibly contaminated by cirrus in the same season.

[22] Over Phimai as indicated in Figure 5a, aerosol is generally more predominant in February and March, while cirrus is more prevailing in April and May. Therefore in order to account for cirrus contamination in aerosol measurements, influences from aerosol seasonal variability need to be further investigated. Additional analysis was conducted by examining data only from April and May when most of biomass burning activities had subsided. Figure 5c compared the probability distribution functions (PDF) of AERONET AOT at Phimai in April 2006, with or without cirrus detected by MPL. A two-sample Kolmogorov-Smirnov (KS) statistical test [*Massey*, 1951], often used for determining the significance level of the difference between

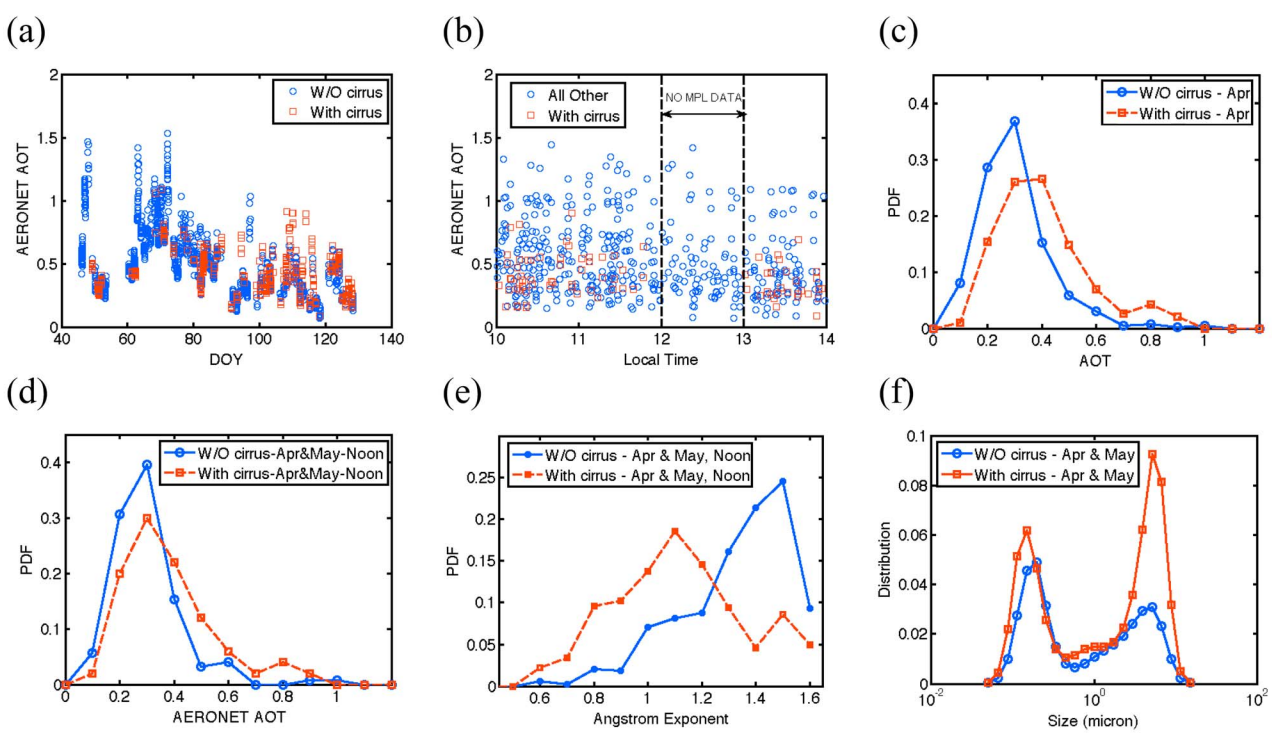

Figure 5. AERONET aerosol products with or w/o cirrus as identified by MPL L1.0 CF: (a) AOT daily variability, (b) AOT diurnal variability, (c) AOT PDF for April only, (d) AOT PDF for local noon hours (1000–1400 local time) in April and May only, (e) Angstrom exponent PDF for local noon hours (1000–1400 local time) in April and May only, and (f) averaged size distribution in April and May only.

Table 2. Changes in the AERONET AOT Means With or Without Cirrus Detected by MPL[a]

AERONET AOT Means	Noncirrus (After Cirrus Screening) (I)	Cirrus-Contaminated (II)	All (Before Cirrus Screening) (III)	Cirrus Screening Impact (%) (IV) = (III-I)/(I)*100	Cirrus Impact (%) (V) = (II-I)/(I)*100
AOT Means Calculated Based on All Sample Means					
BASE-ASIA	0.5209 (1371)	0.4247 (439)	0.4980	−4.38%	−18.5%
BASE-ASIA, noon	0.5291 (439)	0.3904 (86)	0.5072	−4.14%	−26.2%
April	0.3014 (392)	0.4041 (189)	0.3350	+11.1%	+34.1%
April, noon	0.2949 (128)	0.3837 (39)	0.3141	+6.49%	+30.1%
April and May, noon	0.3061 (155)	0.3740 (52)	0.3225	+5.36%	+22.2%
AOT Means Calculated Based on Daily Means					
BASE-ASIA	0.4975	0.4574	0.5077	+2.04%	−8.05%
BASE-ASIA, noon	0.5227	0.3924	0.5204	−0.45%	−24.94%
April	0.3386	0.3920	0.3692	+9.03%	+15.77%
April, noon	0.3405	0.3762	0.3695	+8.52%	+10.48%
April and May, noon	0.3456	0.3685	0.3628	+4.99%	+6.63%

[a]The numbers in the parentheses in the noncirrus and cirrus-contaminated columns are sample sizes of corresponding noncirrus and cirrus-contaminated cases, respectively.

two data distributions, indicates that the two PDFs are significantly different at 95% confidence level. When AOT is contaminated by cirrus, its PDF shifts to higher end, indicating more frequent observations of higher AOT values. This PDF shift reflects that AOT values were biased high when cirrus clouds were miscounted as aerosols. Such overestimation is quantified in Table 2 to be discussed below.

[23] Although cirrus can be persistent throughout the day (Figure 5b), viewing geometry issue should be carefully considered because the micropulse lidar is pointed vertically to the sky (zenith angle = 0°) for aerosol and cloud detection, while the CIMEL Sun photometer is looking toward the sun for AOT retrieval. To minimize the influence from such viewing geometry differences, we further compared the PDFs of the AERONET AOT with or without cirrus by only using the MPLNET and AERONET data retrieved around local noontime (1000–1400 local time) when the viewing angles of two instruments are fairly close with solar zenith angle less than 30°. However, the MPL was shutdown around solar noon to avoid sunlight from entering the telescope (see MPL data gap in Figure 5b). To increase sample size, the noontime data in both April and May were used and their PDFs with or without cirrus contamination were compared in Figure 5d. The PDF shifting to higher AOT values is still significant at 95% confidence level as determined by corresponding K-S analysis.

[24] Because cirrus cloud particle size is generally larger than aerosol particle size, cirrus contamination in the AERONET AOT measurements was examined for changes in mean particle size. We compared the PDFs of the AERONET Angstrom exponents between cases with and without cirrus. Results show that AERONET Angstrom exponents decreased correspondingly when cirrus clouds were detected in the concurrent MPLNET measurements (Figure 5e). Consistently, more large particles were observed in the mean particle size for the cirrus cases than for the noncirrus cases (Figure 5f). Both changes in Angstrom exponent and size distribution further illustrate the cirrus effects in the AERONET aerosol measurements. When the aerosol retrievals miscount cirrus as aerosols, the more cirrus contamination, the more large particles to be observed (Figure 5f), and the smaller the Angstrom exponent is (Figure 5e).

[25] AOT overestimation can be further quantified by calculating 'cirrus impact %' and 'cirrus screening impact %.' The 'cirrus impact %' is defined as

$$\text{Cirrus Impact } \% = \left(\text{AOT}_{\text{with cirrus}} - \text{AOT}_{\text{without cirrus}}\right) / \text{AOT}_{\text{without cirrus}} \times 100,$$

where $\text{AOT}_{\text{with cirrus}}$ and $\text{AOT}_{\text{without cirrus}}$ are AOT means with and without cirrus contamination, respectively. A positive 'cirrus impact %' indicates AOT overestimation caused by cirrus contamination. The 'cirrus screening impact %' is defined as

$$\text{Cirrus Screening Impact } \% = \left(\text{AOT}_{\text{before screening}} - \text{AOT}_{\text{after screening}}\right) / \text{AOT}_{\text{after screening}} \times 100,$$

where $\text{AOT}_{\text{before screening}}$ and $\text{AOT}_{\text{after screening}}$ are AOT means before and after cirrus screening. A positive 'cirrus screening impact %' indicates the effectiveness of cirrus screening that overcomes the AOT overestimation caused by cirrus contamination.

[26] Seen in the first two rows in Table 2, using all data from the BASE-ASIA period by neglecting aerosol seasonality did not show the AOT overestimation caused by cirrus contamination: both the 'cirrus screening impact %' and the 'cirrus impact %' are negative. This is because over the whole campaign period cirrus cases occurred more frequently in low-aerosol months while noncirrus cases were more frequently observed in high-aerosol months (Figure 5a). In contrast, results from using the April-only, Apr-noon-only, and April–May-noon-only data sets all have demonstrated the AOT overestimation: both the 'cirrus screening impact %' and the 'cirrus impact %' are positive. When only the noontime data in April and May were used, the 'cirrus screening impact %' is only 5.36%. This demonstrates the effectiveness of the current operational cloud screening schemes in the AERONET retrievals. However, the corresponding 'cirrus impact %' in cirrus-contaminated cases are on average larger by 22.2%. We also calculated another set of AERONET AOT means that are averages of daily means. The corresponding cirrus screening impact % is ~5% and the cirrus impact percentage is ~7% (see Table 2). Therefore, while it is noteworthy that the current

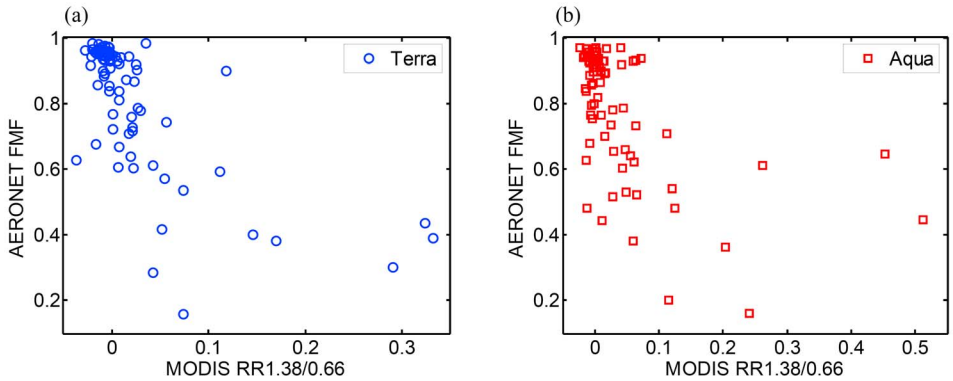

Figure 6. The AERONET L2.0 fine mode fraction as a function of the MODIS-derived reflectance ratio between 1.38 ηm and 0.66 ηm: (a) Terra and (b) Aqua.

AERONET cloud screening scheme seems effectively eliminate most of cloud contaminations, the residual thin cirrus contamination in the AERONET AOT measurements during the BASE-ASIA period is nonnegligible. Thus AOT data with possible cirrus contamination should be carefully screened before they are used for further radiative forcing or other climate impact evaluations.

3.3.2. AERONET Versus CALIPSO

[27] As another independent statistical analysis, we paired up the AERONET AOT with the concurrent CALIPSO cirrus identification by taking advantage of the continuing AERONET data acquisition at Phimai after the completion of the BASE-ASIA campaign. Because of its 16 day observational cycle, during the 2 years of data period between June 2006 and September 2008, only 92 CALIPSO tracks overpass the 1° × 1° grid centered at Phimai. Along these tracks, we selected the cirrus condition at the nearest CALIPSO footprint to represent the regional cirrus condition at Phimai. Overall, 63 (68.5%) out of these 92 days were found with cirrus.

[28] The AERONET AOT data were matched up with the CALIPSO cirrus conditions if the data were collected within 1 h time window centered at the CALIPSO overpass time. In the 48 CALIPSO-AERONET matching-up days, 15 (31.2%) of them were found with cirrus. AOT were elevated from an average of 0.38 under clear sky conditions to 0.45 under cirrus contamination, a 15.9% increase.

3.3.3. AERONET Versus MODIS

[29] As benchmarks for satellite aerosol retrieval validations, cloud screening for AERONET aerosol retrievals around satellite overpass time is crucial. Therefore, it is also of great interest to investigate the potential effects of cirrus on the AERONET retrievals during MODIS overpass. Because the reflectance ratio between 1.38 μm and 0.66 μm (RR1.38/0.66) is indicative of thin cirrus [*Roskovensky and Liou*, 2003], a relationship of the AERONET aerosol Fine Mode Fraction (FMF) to the MODIS-derived RR1.38/0.66 was closely examined. In the spatial context, the matching up RR1.38/0.66 has to be derived from the MODIS pixels that are within 1 km distance from Phimai; in the temporal context, the matching up AERONET FMF data points are selected as the minimum FMF in the 2 h window centered at the MODIS overpass time. This part of study was conducted for both Terra and Aqua in 2006.

[30] Figure 6 shows significant decreases in the AERONET FMF as the MODIS RR1.38/0.66 values increase, particularly when the RR1.38/0.66 is less than 0.2 where thin cirrus contamination most likely occurs. In the 233 matchups for Terra cases (177 for Aqua), there are 21 points (~9%) with RR1.38/0.66 higher than 0.1 (19 points and 11% for Aqua). This relationship between the AERONET FMF and the MODIS RR1.38/0.66 also shed some light on the possible operational routines that can crosscheck AERONET retrievals and operational satellite derived thin cirrus parameters for thin cirrus screening or possible cirrus effect correction in the AERONET aerosol retrievals. Such practice is also crucial for field campaigns that in situ measurements and actual field observations can be linked to satellite observations for environment verification and data validation promptly.

3.3.4. MODIS Versus CALIPSO

[31] Because CALIPSO did not cover the BASE-ASIA period, we investigated a four-season cycle of December 2006 to November 2007 instead. We first retrieved the cirrus information from the CALIPSO VFM at each CALIPSO footprint, and then we matched up such cirrus information with the simultaneous MODIS aerosol retrievals from the nearest MODIS pixel. The best quality MODIS AOT data with quality flags equal to 3 were used. We limited the distance between the central positions of CALIPSO pixel and the closest MODIS pixel to be less than 5 km considering the 10 km resolution of the MODIS AOT product.

[32] During December 2006 to November 2007, there are 4232 all QA (QA > 0) MODIS AOT values collocated with CALIPSO signals over a 5° × 5° grid centered at Phimai, 1907 out of which (45.1%) were found with thin cirrus. Although within the 10 km resolution pixel, cirrus signal may not necessarily be from the exact location where aerosol signals were calculated at 1 km resolution, this percentage at least indicates that MODIS AOT are highly susceptible to residual thin cirrus contamination. This susceptible thin cirrus contamination percentage becomes 59.1% (189/320) when all best quality (QA = 3) MODIS AOT retrievals were evaluated.

[33] Because the MODIS aerosol retrieval is reported at 10 km by aggregating the 1 km resolution pixels, it is difficult to confidently match CALIPSO cirrus pixels with the actual MODIS 1 km pixels that were used in the MODIS

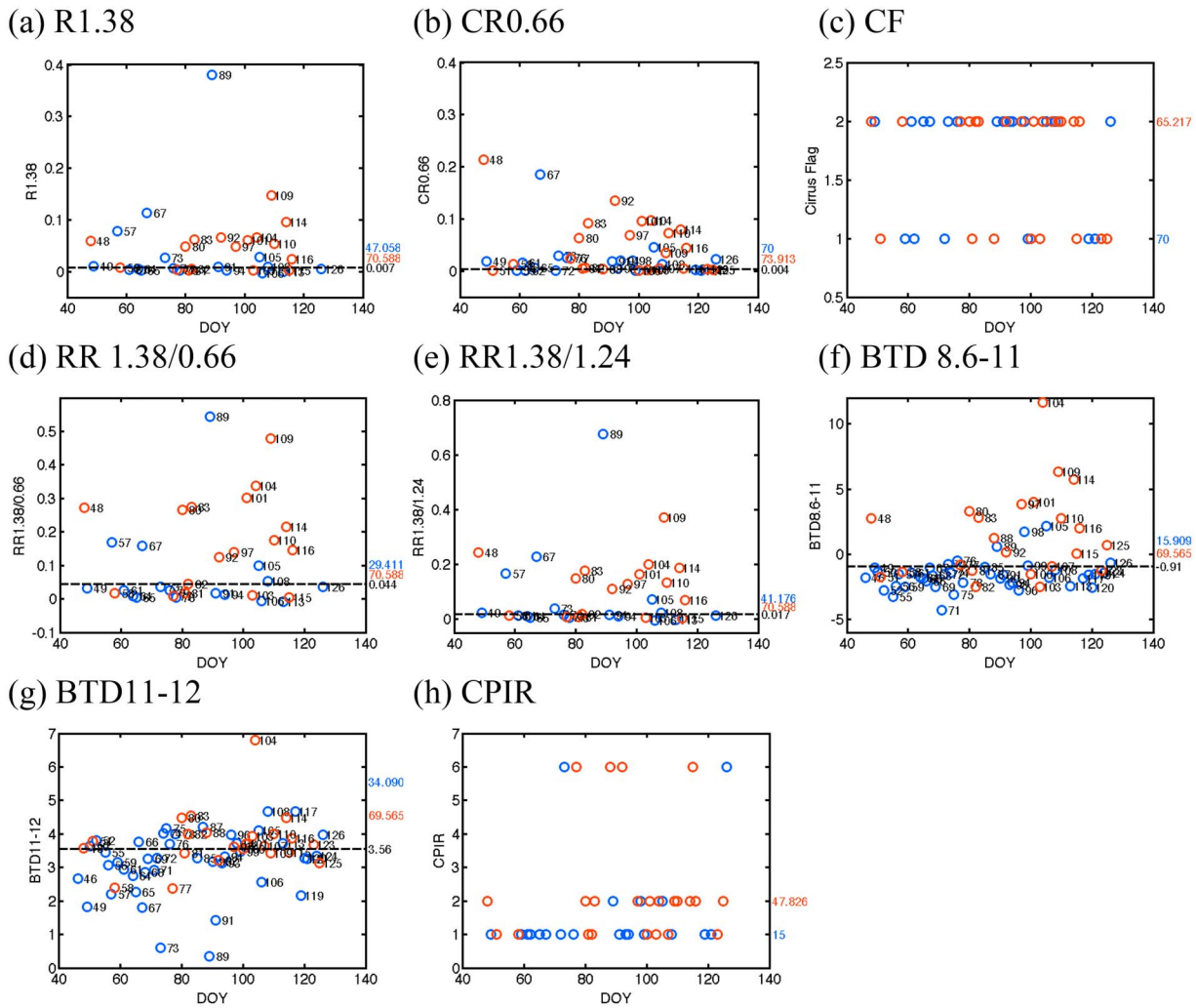

Figure 7. Cirrus screening performances of various MODIS-derived parameters: (a) R1.38 (Uncertainty index <15), (b) CR 0.66 (CF is not bad data), (c) CF, (d) RR1.38/0.66 (R1.38 uncertainty index <15), (e) RR1.38/1.24 (R1.38 uncertainty index <15), (f) BTD 8.6–11, (g) BTD 11–12, and (h) CPIR. Cirrus dates are red circles, and noncirrus dates are blue circles. The numbers on the right-hand side *y* axis denote the threshold value that achieves cirrus identification percent as close to 67% (in black, if the parameter is not flag based), the corresponding cirrus identification percent (in red), and the corresponding noncirrus misidentification percent (in blue).

10 km aerosol products. Consequently, we also examine the MODIS AOT products with both best quality (QA = 3) and zero cloud fraction within the 10 km × 10 km pixels. It is found that 50.6% (84/166) of the "cloud fraction 0" pixels contain thin cirrus and thus 26.3% (84/320) of the best quality pixels are actually cloud contaminated, according to the CALIPSO data. In addition, the best quality (QA = 3) MODIS AOT average during this 1 year period increased by 6.98% from an AOT average of 0.353 for all noncirrus cases to 0.377 for all cirrus-contaminated cases. The Aqua MODIS AOT in cirrus cases tends to be higher than that in noncirrus cases, indicating a possible thin cirrus contamination.

3.4. Evaluations of MODIS-Derived Cirrus Screening Parameters

[34] Another important objective of this study is to find appropriate cirrus screening parameter from operational satellite such as MODIS. Using MPLNET as a benchmark, we matched up MODIS cirrus-screening parameters with MPLNET profiles at MODIS overpass times to evaluate the performances of the MODIS derived cirrus mask. In the 82 day BASE-ASIA campaign period, 69 days had MPL measurements during MODIS overpasses. There are 19 days (27.5%) out of these 69 days that MPLNET detected the presence of cirrus. This further indicated the high probability of cirrus contamination in the MODIS AOT results.

[35] The eight paired up MODIS-derived parameters are R1.38, CR0.66, CF, RR1.38/0.66, RR1.38/1.24, BTD8.6–11, BTD11–12 and CPIR. In general for each parameter that are not flag-based, we set two criteria for threshold value selection: first, the threshold value has to maximize the cirrus identification percentage for cirrus cases; second, the threshold value has to minimize the noncirrus misidentification percentage to avoid miscounting noncirrus cases as

Table 3. MODIS-Derived Cirrus-Screening Parameters and Their Robustness Testing

	Threshold Value	Cirrus Identification (%)	Noncirrus Misidentification (%)
R1.38	0.007	70.6	47.1
CR0.66	0.004	73.9	70.0
CF	2	65.2	70.0
RR1.38/0.66	0.044	70.6	29.4
RR1.38/1.24	0.017	70.6	41.2
BTD8.6–11	−0.91	69.6	15.9
BTD11–12	3.56	69.6	34.1
CPIR	2,4	47.8	15.0

cirrus cases. For example, a threshold value of R1.38 = 0.04 can identify 10 out of 17 cirrus cases (after uncertainty index filtering) with 7 thin cirrus cases missing, and at the same time it also misclassified 3 (DOY57, 67 and 89) out of 17 noncirrus cases as cirrus cases.

[36] In Figure 7 and Table 3, threshold values of each parameter are determined by setting the cirrus identification percentage at 66.7% except CF and CPIR that are flag-based. For CF, cirrus clouds are flagged if CF equals to 2. For CPIR, cirrus clouds are flagged if CPIR values equals to 2 (opaque ice clouds) or 4 (transparent ice clouds).

[37] R1.38, the parameter that is currently used in the operational MODIS cirrus screening scheme, achieves a thin cirrus identification percentage as high as 71% with a threshold value of 0.007. This signifies its effectiveness in cirrus detection. However, with the same threshold value it also overscreens 47% of noncirrus cases. The parameters that identify more than two thirds of cirrus cases while misidentifying less than one third of noncirrus cases are RR1.38/0.66 and BTD8.6–11. With a threshold value of 0.044, RR1.38/0.66 achieved the highest percentage of cirrus identification percentage (71%) with a noncirrus misidentification percentage of 29%. With this threshold value, it also successfully identifies the thin cirrus case of DOY 82 (23 March 2006) in Figure 4. BTD8.6–11 is also effective by identifying 70% of the cirrus cases and misidentifying only 16% of noncirrus cases with its threshold value of −0.91. But as demonstrated in Figure 4, if cirrus layer is as thin as the Phimai case on DOY 82 (Mar 23, 2006), BTD8.6–11 is not sensitive enough to detect such thin cirrus clouds with little ice content. For example, RR1.38/0.66 for DOY 82 is 0.0443 (>0.044) but its BTD8.6–11 is −2.5 (< −0.91). Nonetheless, it might help to minimize noncirrus misidentification if the strengths of RR1.38/0.66 and BTD8.6–11 can be jointly used, as also independently suggested by *Roskovensky and Liou* [2003]. In contrast, although it achieves a similar 70% of cirrus identification percentage and successfully identifies the cirrus case on DOY 82, BTD11–12 misidentifies 34% of the noncirrus cases. Because RR1.38/0.66 and BTD8.6–11 (or 11–12) detect thin cirrus on different theoretical basis, the former is due to the strong water vapor absorption at 1.38 μm and the latter is due to its sensitivity to ice content, a combination is necessary if the first selected parameter fails to detect thin cirrus. For example, when columnar water vapor is too low, R1.38 can penetrate the atmosphere and 'see' ground surface or aerosol/cloud activities in lower troposphere. Thus R1.38, RR1.38/0.66, and RR1.38/1.24 become less reliable for thin cirrus screening because of their potential overscreening. In such water vapor stratification cases, an alternative use of BTD8.6–11 or BTD11–12 should be considered. However, without water vapor stratification or other theoretical considerations, a combination of two or three parameters does not necessarily reduce the misidentification percentage. For Phimai cases, we further tested the following four combinations: RR1.38/0.66 AND/OR BTD8.6–11, RR1.38/0.66 AND/OR BTD11–12. Threshold values were chosen for each within their reasonable data range. The lowest misidentification rate from all these combinations is still as high as 31% while maintaining a 66.7% cirrus identification percentage, not as competitive to using RR1.38/0.66 or BTD8.6–11 alone, although it is worthwhile to emphasize that the results are limited to Phimai cases only.

[38] CF also identified 65% of the cirrus cases, but its misidentification percentage is as high as 70%, which means it might be too aggressive while being used for cirrus screening. RR1.38/1.24 achieved 71% cirrus identification percentage and 41% noncirrus misidentification percentage with a threshold value of 0.017. However, it is noteworthy that, although R1.38 is not sensitive to land and ocean surface features (except total columnar water vapor is very low), R1.24 is significantly higher over land than over ocean. Therefore, the threshold value for RR1.38/1.24 over land and over ocean should be treated differently if the RR1.38/1.24 is employed for cirrus screening purposes. CPIR can flag opaque ice clouds (value 2) and transparent ice clouds (value 4) separately and it achieves the lowest noncirrus misidentification percentage of 15%, however its cirrus identification percentage is only 48%.

4. Summary

[39] The advantageous aerosol and cloud vertical profile detection capabilities from the ground micropulse lidar (MPLNET) and the spaceborne lidar (CALIOP) onboard CALIPSO provide us unprecedented opportunity to systematically examine the susceptibility of ground and satellite AOT measurements to cirrus clouds, which is currently a major challenge for most of cloud screening schemes in aerosol retrieval algorithms. Based on the observational data sets from the BASE-ASIA campaign and the A-Train satellites, we conducted comprehensive evaluations on the effects of possible cirrus contaminations in the susceptible aerosol measurements.

[40] Several points learned from this study were outlined as follows. First of all, the ground AOT measurements from CIMEL Sun photometer at the BASE-ASIA campaign were susceptible to cirrus contamination, particularly over April and May time period. Overall, MPLNET measurements observed concurrent cirrus occurrences in 24% of the AERONET aerosol data in boreal spring, but with strong seasonal variability. Second, data from BASE-ASIA campaign show that the monthly mean AERONET AOT may only be improved by ~5% if additional cirrus screening technique is implemented, indicating the effectiveness of the current operational cloud screening schemes in the AERONET L2.0 aerosol retrievals. However, for PDF comparisons of cirrus-contaminated cases with noncirrus cases,

increased AOT and more population of large particles were apparently observed in the AERONET aerosol retrievals. Thus, it is imperative to identify the presence of cirrus in the ground based AOT and Angstrom exponent measurements or have cirrus effect taken into account before they can be used for further climatic forcing analysis so that any exaggerated overestimation can be avoided.

[41] We also tested 8 different MODIS-derived cirrus-screening parameters for their performance on cirrus identification against cirrus flags from the MPLNET observations. Overall, the reflectance ratio RR1.38/0.66 between two channels at 1.38 μm and 0.66 μm achieves relatively better cirrus identification percentage and smaller misidentification percentage than others. Selecting an optimal MODIS-derived thin cirrus screening parameter is not only important for MODIS operational aerosol retrievals, but also valuable for evaluating AERONET aerosol retrievals on daily basis, particularly when the AERONET site is not close enough to CALIPSO tracks or MPL lidar is not available for AERONET site. Although polar orbiting satellites such as Terra and Aqua do not provide temporal coverage of cirrus information over the entire diurnal cycle needed for the AERONET measurements, such cirrus screening derived from MODIS could serve as an important piece of puzzle in interpreting the results of AERONET-satellite collocation related studies, such as the satellite aerosol retrieval validation efforts.

[42] While the susceptibility of aerosol products to thin cirrus contamination during the BASE-ASIA campaign was demonstrated, we believe a global survey of the issue will provide more valuable assets to deepening our comprehensive and quantitative understanding on the data uncertainty in global aerosol products caused by thin cirrus contamination. Future work on the susceptibility of aerosol products to thin cirrus at a global view is currently underway.

[43] **Acknowledgments.** This work is supported by a grant from the NASA EOS Program, managed by Hal Maring. The authors thank Alexander Smirnov, David Giles, Bo-Cai Gao, Richard A. Hansell, Steve Ou, and Zhien Wang for their constructive comments on the use of in situ and satellite data, analysis methodology, and cirrus climatology. The authors thank three anonymous reviewers for their comments that were valuable to improving the paper. Aqua MODIS L1B and L2 data were obtained from NASA L1 and Atmosphere Archive and Distribution System (LAADS). CALIPSO data were obtained from the NASA Langley Research Center Atmospheric Science Data Center.

References

Andreae, M. O. (1991), Biomass burning: Its history, use, and distribution and its impact on environmental quality and global change, in *Global Biomass Burning: Atmospheric, Climatic. and Biospheric Implications*, edited by J. S. Levine, pp. 3–21, MIT Press, Cambridge, Mass.

Berkoff, T., Q. Ji, R. Kleidman, S. Stewart, E. J. Welton, Z. Li, and B. Holben (2008), Ground-based lidar measurements during the CALIPSO and Twilight Zone (CATZ) campaign, *Eos Trans. AGU*, *88*(23), Spring Meet. Suppl., Abstract A33D-14.

Breon, F.-M., D. Tanre, and S. Generso (2002), Aerosol effect on cloud droplet size monitored from satellite, *Science*, *295*, 834–838, doi:10.1126/science.1066434.

Chu, D. A., Y. J. Kaufman, J.-D. Chern, G. Zibordi, J. Mao, C. Li, and H. B. Holben (2003), 2002: Global monitoring of air pollution over land from EOS-Terra MODIS, *J. Geophys. Res.*, *108*(D21), 4661, doi:10.1029/2002JD003179.

Gao, B. C., and Y. Kaufman (1995), Selection of the 1.375 μm MODIS channel for remote sensing of cirrus clouds and stratospheric aerosols from space, *J. Atmos. Sci.*, *52*, 4231–4237, doi:10.1175/1520-0469(1995)052<4231:SOTMCF>2.0.CO;2.

Gao, B. C., Y. Kaufman, D. Tanre, and R.-R. Li (2002a), Distinguishing tropospheric aerosols from thin cirrus clouds for improved aerosol retrievals using the ratio of 1.38-μm and 1.24-μm channels, *Geophys. Res. Lett.*, *29*(18), 1890, doi:10.1029/2002GL015475.

Gao, B. C., P. Yang, W. Han, R.-R. Li, and W. J. Wiscombe (2002b), An algorithm using visible and 1.38-μm channels to retrieve cirrus cloud reflectances from aircraft and satellite data, *IEEE Trans. Geosci. Remote Sens.*, *40*, 1659–1668, doi:10.1109/TGRS.2002.802454.

Hansell, R. A., S.-C. Tsay, Q. Ji, K. N. Liou, and S. C. Qu (2003), The surface aerosol radiative forcing derived from collocated ground-based radiometric observations during PRIDE, SAFARI, and ACE-ASIA and at UCLA site, *Appl. Opt.*, *42*, 5533–5544, doi:10.1364/AO.42.005533.

Holben, B. N., et al. (1998), AERONET—A federated instrument network and data archive for aerosol characterization, *Remote Sens. Environ.*, *66*, 1–16, doi:10.1016/S0034-4257(98)00031-5.

Hsu, N. C., J. R. Herman, P. K. Bhartia, C. J. Seftor, O. Torres, A. M. Thompson, J. F. Gleason, T. F. Eck, and B. N. Holben (1996), Detection of biomass burning smoke from TOMS measurements, *Geophys. Res. Lett.*, *23*, 745–748, doi:10.1029/96GL00455.

Hsu, N. C., J. R. Herman, and S.-C. Tsay (2003), Radiative impacts from biomass burning in the presence of clouds during boreal spring in southeast Asia, *Geophys. Res. Lett.*, *30*(5), 1224, doi:10.1029/2002GL016485.

Hsu, N. C., S. C. Tsay, M. D. King, and J. R. Herman (2006), Deep blue retrievals of Asian aerosol properties during ACE-Asia, *IEEE Trans. Geosci. Remote Sens.*, *44*, 3180–3195, doi:10.1109/TGRS.2006.879540.

Jeong, M. J., and Z. Li (2005), Quality, compatibility and synergy analyses of global aerosol products derived from the advanced very high resolution radiometer and total ozone mapping spectrometer, *J. Geophys. Res.*, *110*, D10S08, doi:10.1029/2004JD004647.

Jeong, M. J., Z. Li, D. A. Chu, and S.-C. Tsay (2005), Quality and compatibility analyses of global aerosol products derived from the advanced very high resolution radiometer and moderate resolution imaging spectroradiometer, *J. Geophys. Res.*, *110*, D10S09, doi:10.1029/2004JD004648.

Kaufman, Y. J., D. Tanré, L. A. Remer, E. F. Vermote, A. Chu, and B. N. Holben (1997), Operational remote sensing of tropospheric aerosol over land from EOS moderate resolution imaging spectroradiometer, *J. Geophys. Res.*, *102*(D14), 17,051–17,067, doi:10.1029/96JD03988.

Kaufman, Y. J., et al. (2005), A critical examination of the residual cloud contamination and diurnal sampling effects on MODIS estimates of aerosol over ocean, *IEEE Trans. Geosci. Remote Sens.*, *43*, 2886–2897, doi:10.1109/TGRS.2005.858430.

Kaufman, Y. J., G. P. Gobbi, and I. Koren (2006), Aerosol climatology using a tunable spectral variability cloud screening of AERONET data, *Geophys. Res. Lett.*, *33*, L07817, doi:10.1029/2005GL025478.

Lee, J., P. Yang, A. Dessler, B.-C. Gao, and S. Platnick (2009), Distribution and radiative forcing of tropical thin cirrus clouds, *J. Atmos. Sci.*, *66*, 3721–3731, doi:10.1175/2009JAS3183.1.

Levine, J. S., et al. (1989), *FireSat and the Global Monitoring of Biomass Burning*, Natl. Res. Counc., Natl. Acad. Press, Washington, D. C.

Li, Z., et al. (2007), Preface to special section on East Asian Studies of Tropospheric Aerosols: An International Regional Experiment (EAST-AIRE), *J. Geophys. Res.*, *112*, D22S00, doi:10.1029/2007JD008853.

Liu, Z., et al. (2009), The CALIPSO lidar cloud and aerosol discrimination: Version 2 algorithm and initial assessment of performance, *J. Atmos. Oceanic Technol.*, *26*, 1198–1213, doi:10.1175/2009JTECHA1229.1.

Luo, C. (2004), A global satellite view of aerosol cloud interactions, *Atmos. Chem. Phys.*, *4*, 6823–6836, doi:10.5194/acpd-4-6823-2004.

Massey, F. J. (1951), The Kolmogorov-Smirnov test for goodness of fit, *J. Am. Stat. Assoc.*, *46*(253), 68–78, doi:10.2307/2280095.

Massie, S. T., J. Gille, C. Craig, R. Khosravi, J. Barnett, W. Read, and D. Winker (2010), HIRDLS and CALIPSO observations of tropical cirrus, *J. Geophys. Res.*, *115*, D00H11, doi:10.1029/2009JD012100.

Menon, S., J. Hansen, L. Nazarenko, and Y. Luo (2002), Climate effects of black carbon aerosols in China and India, *Science*, *297*, 2250–2253, doi:10.1126/science.1075159.

Meyer, K., and S. Platnick (2010), Utilizing the MODIS 1.38 μm channel for cirrus cloud optical thickness retrievals: Algorithm and retrieval uncertainties, *J. Geophys. Res.*, *115*, D24209, doi:10.1029/2010JD014872.

Myhre, G., et al. (2005), Intercomparison of satellite retrieved aerosol optical depth over ocean during the period September 1997 to December 2000, *Atmos. Chem. Phys.*, *5*, 1697–1719, doi:10.5194/acp-5-1697-2005.

Roskovensky, J. K., and K. N. Liou (2003), Detection of thin cirrus from 1.38 mm/0.65 mm reflectance ratio combined with 8.6–11 mm brightness temperature difference, *Geophys. Res. Lett.*, *30*(19), 1985, doi:10.1029/2003GL018135.

Sassen, K., Z. Wang, and D. Liu (2008), Global distribution of cirrus clouds from CloudSat/Cloud-Aerosol Lidar and Infrared Pathfinder

Satellite Observations (CALIPSO) measurements, *J. Geophys. Res.*, *113*, D00A12, doi:10.1029/2008JD009972.

Schaap, M., A. Apituley, R. M. A. Timmermans, R. B. A. Koelemeijer, and G. de Leeuw (2009), Exploring the relation between aerosol optical depth and $PM_{2.5}$ at Cabauw, the Netherlands, *Atmos. Chem. Phys.*, *9*, 909–925, doi:10.5194/acp-9-909-2009.

Smirnov, A., B. N. Holben, T. F. Eck, O. Dubovik, and I. Slutsker (2000), Cloud-screening and quality control algorithms for the AERONET database, *Remote Sens. Environ.*, *73*, 337–349, doi:10.1016/S0034-4257(00)00109-7.

Takemura, T., T. Nozawa, S. Emori, T. Y. Nakajima, and T. Nakajima (2005), Simulation of climate response to aerosol direct and indirect effects with aerosol transport-radiation model, *J. Geophys. Res.*, *110*, D02202, doi:10.1029/2004JD005029.

Tao, W.-K., X. Li, A. Khain, T. Matsui, S. Lang, and J. Simpson (2007), Role of atmospheric aerosol concentration on deep convective precipitation: Cloud-resolving model simulations, *J. Geophys. Res.*, *112*, D24S18, doi:10.1029/2007JD008728.

Unger, N., S. Menon, D. M. Koch, and D. T. Shindell (2009), Impacts of aerosol-cloud interactions on past and future changes in tropospheric composition, *Atmos. Chem. Phys.*, *9*, 4115–4129, doi:10.5194/acp-9-4115-2009.

Vaughan, M. A., S. A. Young, D. M. Winker, K. A. Powell, A. H. Omar, Z. Liu, Y. Hu, and C. A. Hostetler (2004), Fully automated analysis of space-based lidar data: An overview of the CALIPSO retrieval algorithms and data products, *Proc. SPIE Int. Soc. Opt. Eng.*, *5575*, 16–30.

Vaughan, M. A., D. M. Winker, and K. A. Powell (2005), CALIOP algorithm theoretical basis document, part 2: Feature detection and layer properties algorithms, *Rep. PC-SCI-202.02*, 87 pp., NASA Langley Res. Cent., Hampton, Va. [Available at http://www-calipso.larc.nasa.gov/resources/project_documentation.php.]

Welton, E. J., J. R. Campbell, J. D. Spinhirne, and V. S. Scott (2001), Global monitoring of clouds and aerosols using a network of micro-pulse lidar systems, *Proc. SPIE Int. Soc. Opt. Eng.*, *4153*, 151–158.

T. A. Berkoff and J. Huang, Goddard Earth Sciences and Technology Center, University of Maryland Baltimore County, 5523 Research Park Dr., Baltimore, MD 21228, USA. (jfhuang@umbc.edu)

B. N. Holben, N. C. Hsu, S.-C. Tsay, and E. J. Welton, NASA Goddard Space Flight Center, Greenbelt, MD 20771, USA.

M.-J. Jeong, Department of Atmospheric and Environmental Sciences, Gangneung-Wonju National University, Gangneung, Gangwon-do 210-702, South Korea.